


Multiple transparency windows and Fano interferences induced by dipole-dipole couplingsE. C. Diniz,^{*} H. S. Borges,[†] and C. J. Villas-Boas[‡]*Departamento de Física, Universidade Federal de São Carlos, P.O. Box 676, 13565-905, São Carlos, São Paulo, Brazil* (Received 21 September 2017; published 19 April 2018)

We investigate the optical properties of a two-level system (TLS) coupled to a one-dimensional array of N other TLSs with dipole-dipole coupling between the first neighbors. The first TLS is probed by a weak field, and we assume that it has a decay rate much greater than the decay rates of the other TLSs. For $N = 1$ and in the limit of a Rabi frequency of a probe field much smaller than the dipole-dipole coupling, the optical response of the first TLS, i.e., its absorption and dispersion, is equivalent to that of a three-level atomic system in the configuration which allows one to observe the electromagnetically induced transparency (EIT) phenomenon. Thus, here we investigate an induced transparency phenomenon where the dipole-dipole coupling plays the same role as the control field in EIT in three-level atoms. We describe this physical phenomenon, named a dipole-induced transparency (DIT), and investigate how it scales with the number of coupled TLSs. In particular, we have shown that the number of TLSs coupled to the main TLS is exactly equal to the number of transparency windows. The ideas presented here are very general and can be implemented in different physical systems, such as an array of superconducting qubits, or an array of quantum dots, spin chains, optical lattices, etc.

DOI: [10.1103/PhysRevA.97.043848](https://doi.org/10.1103/PhysRevA.97.043848)**I. INTRODUCTION**

Understanding of light-matter interaction has been the focus of intense research during the last decades, mainly due to advances in its manipulation allowed by the introduction of laser fields. Many of these efforts are justified in view of the possibility of using it for the implementation and control of quantum systems in a variety of areas, including quantum computing [1,2], collective atomic phenomena [3], trapped ions [4], cavity and circuit QED [5,6], and other applications involving microscopic scales. Despite the difficulties related to the control and implementation of coupled quantum systems, which are essential for building scalable quantum networks [7], significant advances have been achieved using some quantum devices in last years; see, for instance, Refs. [5–7], which are some examples of physical systems where one finds high control either of light-matter or matter-matter interactions, which are essential for the implementation of our proposal as discussed later. In this sense, electromagnetically induced transparency (EIT) [8,9] has been shown to be a phenomenon very useful for manipulating light with light, allowing many applications, such as in optical transistors [10,11], quantum memories [12,13], to generate controllable phase shifts on single-photon pulses [14], or ground-state cooling of either single atoms [15,16] or ion strings [17], among many others. Thus, the investigation of other physical systems which present EIT-related phenomenon could open new possibilities for the implementation of such applications.

The first systematic experimental studies of EIT were carried out with three-level atoms in Λ configuration [8]. Since the appearance of the work by Boller *et al.* [8], the fundamental

idea of EIT has been extended to other systems. Now one can observe the interference between different absorption pathways, resulting in adjustable transparency windows, in a large variety of different physical systems, such as in coupled classical [18] or quantum harmonic oscillators [19], two-coupled optical cavity modes [20,21], a two-level atom coupled to a cavity mode [22,23], quantum dot molecules [24–26], plasmonic systems [27,28], optomechanical oscillators [29,30], metamaterials [31,32], etc. By applying more control fields and involving additional ground states, more transparency windows can be obtained, thus revealing the double-EIT phenomenon [33,34]. Double-transparency windows can also be observed in multiple coupled photonic crystal cavities [35] or in optomechanical systems [36]. These ideas can also be extended to multiple transparency windows, which can be achieved either in $(N + 1)$ -level atomic systems [37] or in N periodically coupled whispering gallery-mode resonators [38].

Here we investigate the optical response of a two-level system (TLS) coupled to a one-dimensional (1D) array of N other TLSs with dipole-dipole coupling between the first neighbors, as schematically shown in Fig. 1. We show that the dipole-dipole coupling plays exactly the same role as the control field in the EIT phenomenon, either in free space [9,21] or in cavity QED experiments [11]. We also investigate the scalability of this system, i.e., how it is possible to control the number of transparency windows.

II. PHYSICAL SYSTEM AND MODEL

We assume a weak probe field with oscillation frequency ω_p , driving only the main TLS, such that the Hamiltonian in the rotating frame of the driving field is given by ($\hbar = 1$)

$$H = \sum_{i=0}^N \frac{\Delta_p \sigma_z^i}{2} + \sum_{i=0}^{N-1} (d_i \sigma_-^i \sigma_+^{i+1} + \text{H.c.}) + \Omega_p (\sigma_+^0 + \text{H.c.}), \quad (1)$$

^{*}ediniz98@gmail.com[†]halyneborges@gmail.com[‡]villasboas@ufscar.br

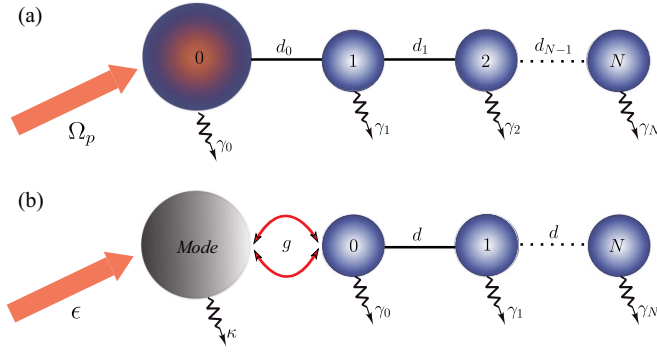


FIG. 1. Pictorial representation of the system: (a) 1 + N coupled two-level systems (TLSs) and (b) a driven cavity mode coupled to 1 + N TLSs.

where $\Delta_p = \omega_0 - \omega_p$. Here $\sigma_z^i = (|e\rangle\langle e|^{(i)} - |g\rangle\langle g|^{(i)})$ and $\sigma_{\pm}^i = (\sigma_{\pm}^i)^{\dagger} = |g\rangle\langle e|^{(i)}$ are the operators (Pauli's matrix) of the i th TLS, with $|e\rangle$ and $|g\rangle$ the excited and ground states, respectively, whose transition frequency is ω_0 . d_i is the dipole-dipole coupling, and $2\Omega_p$ is the Rabi frequency of the probe field. The above Hamiltonian can be found or engineered in a large variety of different physical systems, such as optical lattices [39,40], in an array of coupled optical cavities with single trapped atoms inside [41], superconducting qubits coupled to two-level systems [42–46], coupled superconducting qubits [47], in a trapped ion domain [48], or in an array of quantum dots [49,50].

A. Dipole-induced transparency in a 1D array of TLSs

Considering the environment at $T = 0$ K and the limits of a weak system-reservoir and weak dipole-dipole ($|d_i| \ll \omega_0$) couplings, the dissipation mechanisms of the whole system can be taken into account via the master equation in Lindblad form [51] $\dot{\rho} = -i[H, \rho] + \mathcal{D}[\rho]$, where $\mathcal{D}[\rho] = \sum_{i=0}^N \gamma_i (2\sigma_{-}^i \rho \sigma_{+}^i - \sigma_{+}^i \sigma_{-}^i \rho - \rho \sigma_{+}^i \sigma_{-}^i)$, γ_i being the decay rate of the i th TLS. We obtain the steady-state solution and then investigate the optical response of the main TLS, which can be derived analytically for an arbitrary number of TLSs in the limit of a weak excitation regime. To this end, we derived the average value $\langle \sigma_{-}^0 \rangle_{ss} = \text{Tr}(\rho_{ss} \sigma_{-}^0)$ in the weak probe field limit, i.e., $|\Omega_p| \ll |d_0|$, and when the decay rate of the main TLS is greater than that of the others, i.e., $\gamma_0 \gg \gamma_i$.

Such assumptions allow us to employ the semiclassical approximation [52]. From this approximation, we find the equations of motion for the expectation values of the system operators where the correlations between atomic operators are neglected, i.e., $\langle \sigma_{\pm}^i \sigma_{\pm}^j \rangle \approx \langle \sigma_{\pm}^i \rangle \langle \sigma_{\pm}^j \rangle$ ($i \neq j$). Based on these assumptions we can derive the general system of equations for the expectation values of the TLS operators:

$$\begin{aligned} \langle \dot{\sigma}_{-}^0 \rangle &= -i(\Delta_p + \gamma_0) \langle \sigma_{-}^0 \rangle + id_0 \langle \sigma_z^0 \rangle \langle \sigma_{-}^1 \rangle + i\Omega_p \langle \sigma_z^0 \rangle, \\ \langle \dot{\sigma}_{-}^j \rangle &= -i(\Delta_p + \gamma_j) \langle \sigma_{-}^j \rangle + id_{j-1} \langle \sigma_z^j \rangle \langle \sigma_{-}^{j-1} \rangle \\ &\quad + id_{j+1} \langle \sigma_z^j \rangle \langle \sigma_{-}^{j+1} \rangle \quad (\text{for } 1 \leq j \leq N-1), \\ \langle \dot{\sigma}_{-}^N \rangle &= -i(\Delta_p + \gamma_N) \langle \sigma_{-}^N \rangle + id_{N-1} \langle \sigma_z^N \rangle \langle \sigma_{-}^{N-1} \rangle. \end{aligned} \quad (2)$$

Considering $\langle \sigma_z^k \rangle \approx -1$ ($k = 0, 1, \dots, N$), from the general motion equations (2), we obtain the general steady-state solution:

$$\langle \sigma_{-}^0 \rangle_{ss} \approx -\Omega_p \frac{\delta_1}{\delta_0} \quad (3)$$

with

$$\delta_k = \delta_{k+1}(\Delta_p - i\gamma_k) - \delta_{k+2}|d_k|^2 \quad (4)$$

for $k = 0, 1, \dots, N-2$, and

$$\delta_{N-1} = \delta_N(\Delta_p - i\gamma_{N-1}) - |d_{N-1}|^2, \quad (5)$$

$$\delta_N = (\Delta_p - i\gamma_N). \quad (6)$$

For some special cases, we can obtain simple expressions for $\langle \sigma_{-}^0 \rangle_{ss}$ (see Appendix A). For instance, considering the main TLS coupled to another single ($N = 1$), in the weak probe field limit we obtain the following steady-state solution:

$$\langle \sigma_{-}^0 \rangle_{ss} = \text{Tr}(\rho_{ss} \sigma_{-}^0) \approx \frac{(\Delta_p - i\gamma_1)\Omega_p}{|d_0|^2 - (\Delta_p - i\gamma_0)(\Delta_p - i\gamma_1)}. \quad (7)$$

From this expression we can promptly derive the dispersion and absorption, its real and imaginary parts, respectively, and then we can analyze the optical response of this system.

Our system, composed by two coupled TLSs, can be compared to the system constituted by two quantum dots with dipole-dipole coupling employed to perform an optical switching [53]. However, different from our system, in [53] the transparency is not induced by the dipole-dipole interaction and the authors assume two fields acting simultaneously on both quantum dots (TLSs) and the same decay rates for them. In this way, they are able to show an efficient optical switching only when the Rabi frequency of the control field is much greater than the decay rate of the quantum dots. In fact, in this regime one has an Autler-Townes (AT) splitting instead of a real interference between different excitation pathways [54], which is the fundamental process behind EIT.

Comparing the linear susceptibility function of our system with those of a three-level atomic system in the EIT regime [9,21], we immediately recognize a kind of induced transparency in which the dipole-dipole coupling d_0 plays the same role as the Rabi frequency of the control field [see Eqs. (A1) and (A2) in Appendix A]. We can also see that the decay rate of the first (second) TLS plays the same role as the total decay rate of the excited state Γ (dephasing rate γ_{ph}) in three-level systems in the EIT regime, which makes clear the requirement for different decay rates for the two TLSs employed in our model. Thus, here we have a *dipole-induced transparency* (DIT) phenomenon. However, it is important to emphasize that despite that the linear optical response of our system and that of the Λ -type three-level system are completely analogous, the nonlinear responses have marked differences. (The analytical expressions of third-order optical susceptibility for both systems are shown in the Appendix A.)

In Fig. 2(a) we plot the imaginary and real parts of $\langle \sigma_{+}^0 \rangle_{ss}$ as a function of Δ_p/γ_0 for a set of parameters which allows the observation of DIT. Keeping $|d_0| \gg |\Omega_p|$ and $|d_0| < \gamma_0$, we can note that the transparency window directly depends on the dipole-dipole coupling d_0 , as expected. In another related work

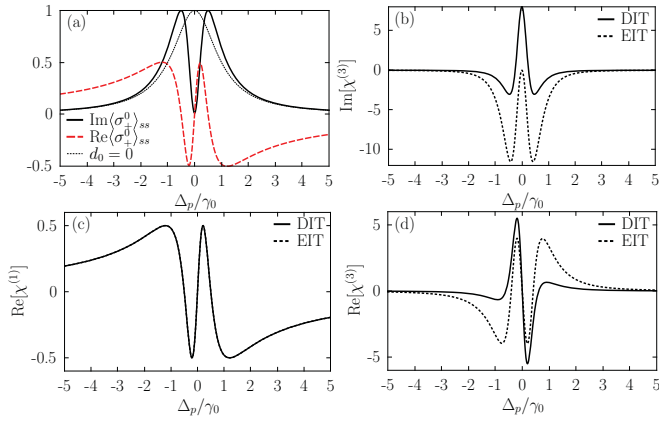


FIG. 2. (a) Normalized absorption (black solid line) and dispersion (red dashed line) of the first TLS when coupled to a second one as a function of Δ_p/γ_0 . The black dotted line represents the absorption when $d_0 = 0$. (b) Imaginary part of the third-order optical susceptibility for two different systems: two TLSs coupled by dipole-dipole interaction (solid line) and a usual three-level system where EIT phenomenon can be observed (dashed line). (c) Real part of the first-order and (d) real part of the third-order optical susceptibility functions for two TLSs coupled by dipole-dipole interaction (solid line) and usual Λ system (dashed line). In (c) the curves overlap perfectly. Parameters used: $\Omega_p = 0.03\gamma_0$, $d_0 = 0.5\gamma_0$, $\gamma_1 = 10^{-3}\gamma_0$.

[55], the authors claim that it is possible to observe a similar effect, i.e., a dipole-induced transparency, in a high-density atomic medium which contains two species of atoms (different dipoles). However, as they assume the same decay rate for both dipoles, they cannot observe an extremely narrow transparency window, as usually allowed in EIT experiments [56]. In order to observe the differences and similarities between the usual EIT phenomenon in three-level atoms in Λ configuration and our DIT in coupled TLSs, in Figs. 2(b)–2(d) we compare the optical susceptibility functions of both systems. In Fig. 2(b) we plot the imaginary part of the third-order optical susceptibility function of both systems (for the same set of parameters) as a function of Δ_p/γ_0 , where it is possible to observe the transparency effect induced by dipole-dipole interaction (solid line) and by a control electromagnetic field in three-level atoms (dashed line). The real part of the first-order and third-order optical susceptibility functions is plotted in Figs. 2(c) and 2(d). These results evidence the difference between the nonlinear optical response of both systems, although their linear optical responses are identical.

B. DIT in a 1D array of TLSs coupled to a resonator

Considering a three-level atom in the EIT configuration and coupled to a cavity mode, one can observe a cavity EIT [11]. According to the discussion above, the same effect should be observed by replacing the three-level atom by two coupled TLSs. This is in fact the case, as we will explain in the following. To this end, let us first describe a more general system, i.e., the interaction of a quantum resonator with a 1D array of $1 + N$ two-level systems, as schematically represented in Fig. 1(b), with dipole-dipole coupling d_i and individual decay rates γ_i . The first TLS is then resonantly coupled to the

cavity mode, coupling g , which is driven by a probe field of strength ϵ and frequency ω_p . The Hamiltonian of this system, written in the rotating frame of the probe field, reads (for $\hbar = 1$)

$$H_c = \Delta_p \left(a^\dagger a + \sum_{i=0}^N \frac{\sigma_z^i}{2} \right) + (\epsilon a + \text{H.c.}) + H_I, \quad (8)$$

with $\Delta_p = \omega_0 - \omega_p = \omega_{cav} - \omega_p$, ω_{cav} being the cavity mode frequency and $H_I = \sum_{i=0}^{N-1} d_i (\sigma_-^i \sigma_+^{i+1} + \text{H.c.}) + g(a \sigma_+^0 + \text{H.c.})$. In this case, the dissipation of the cavity mode can be taken into account by adding the term $\kappa(2a\rho a^\dagger - a^\dagger a \rho - \rho a^\dagger a)$ into the master equation of the system, with κ the decay rate of the cavity field amplitude. This new master equation can also be analytically solved for some particular set of parameters, as we show in the following.

Employing the semiclassical approximation [52], which allows us to factorize the correlator $\langle a \sigma_-^i \rangle \approx \langle \sigma_-^i \rangle \langle a \rangle$, we obtain the analytical solution for the average value of the annihilation operator of the cavity mode for the $1 + N$ coupled TLS case. This semiclassical approach is a good approximation whenever the driving field is very weak compared to the dissipation rate of the cavity mode and the atom-field coupling is also not so strong (again, when compared to the cavity field decay rate κ).

The derivation of the steady-state solution for $\langle a \rangle$ and arbitrary number of TLSs coupled to a resonator follows the recurrence relations for the equations of motion for the average value of the atomic or resonator operators:

$$\begin{aligned} \langle \dot{a} \rangle &= -i(\Delta_p - i\kappa)\langle a \rangle - ig\langle \sigma_-^0 \rangle - i\epsilon, \\ \langle \dot{\sigma}_-^0 \rangle &= -i(\Delta_p - i\gamma_0)\langle \sigma_-^0 \rangle + ig\langle a \rangle \langle \sigma_z^0 \rangle + id_0 \langle \sigma_z^0 \sigma_-^1 \rangle, \\ \langle \dot{\sigma}_-^j \rangle &= -i(\Delta_p - i\gamma_j)\langle \sigma_-^j \rangle + id_{j-1} \langle \sigma_z^j \sigma_-^{j-1} \rangle \\ &\quad + id_j \langle \sigma_z^j \sigma_-^{j+1} \rangle, \quad (\text{for } 1 \leq j \leq N-1) \\ \langle \dot{\sigma}_-^N \rangle &= -i(\Delta_p - i\gamma_N)\langle \sigma_-^N \rangle + id_{N-1} \langle \sigma_z^N \sigma_-^{N-1} \rangle. \end{aligned} \quad (9)$$

From this coupled equation system we can derive the stationary solution of $\langle a \rangle_{ss}$ for an arbitrary number of TLSs coupled to the cavity mode. Following a similar procedure used to obtain the optical response of the 1D array of TLSs in free space, here we can write the expectation values of $\langle a \rangle$ and $\langle \sigma_\pm^k \rangle$. Thus, considering again $\langle \sigma_z^k \rangle \approx -1$ ($k = 0, 1, \dots, N$), we obtain from the general motion equations (9) the following general expected value:

$$\langle a \rangle_{ss} \approx -\epsilon \frac{\delta_0}{\delta_c}, \quad (10)$$

with

$$\delta_c = \delta_0(\Delta_p - i\kappa) - \delta_1 |g|^2, \quad (11)$$

$$\delta_k = \delta_{k+1}(\Delta_p - i\gamma_k) - \delta_{k+2} |d_k|^2, \quad (12)$$

for $k = 0, 1, \dots, N-2$, and

$$\delta_{N-1} = \delta_N(\Delta_p - i\gamma_{N-1}) - |d_{N-1}|^2, \quad (13)$$

$$\delta_N = (\Delta_p - i\gamma_N). \quad (14)$$

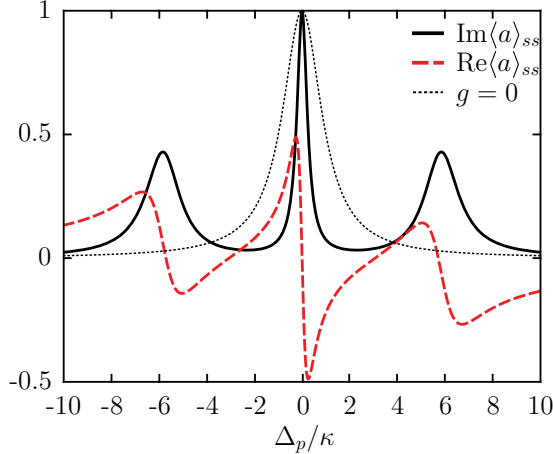


FIG. 3. Normalized absorption $\text{Im}\langle a \rangle_{ss}$ (black solid line) and dispersion $\text{Re}\langle a \rangle_{ss}$ (red dashed line) of the cavity mode when coupled to two-coupled TLSs as a function of the normalized detuning Δ_p/κ . Parameters used: $\gamma_0 = \kappa$, $g = 5\kappa$, $d = 3\kappa$, $|\epsilon| = 0.03\kappa$, and $\gamma_1 = 10^{-3}\kappa$. The black dotted lines represent the absorption when there is no TLS coupled to the cavity mode ($g = 0$).

For instance, for $N = 1$ (two coupled TLSs coupled to the cavity mode), the steady-state solution reads

$$\langle a \rangle_{ss} = \frac{\epsilon d^2 - \epsilon(\Delta_p - i\gamma_0)(\Delta_p - i\gamma_1)}{-g^2(\Delta_p - i\gamma_1) - d_0^2(\Delta_p - i\kappa) + \Psi}, \quad (15)$$

where $\Psi = (\Delta_p - i\gamma_0)(\Delta_p - i\gamma_1)(\Delta_p - i\kappa)$. This equation must be compared to the equation for the average value of the annihilation operator for a cavity mode coupled to a three-level atom in the EIT configuration (cavity-EIT) [21]. In Fig. 3 we plot the normalized absorption and dispersion of the cavity mode when coupled to two coupled TLSs, here defined as $\text{Im}\langle a \rangle_{ss}$ and $\text{Re}\langle a \rangle_{ss}$, respectively.

III. SCALABILITY OF THE SYSTEM: MULTIPLE DIT

The results above can be properly extended to multiple transparency windows by adding more TLSs, as schematically shown in Fig. 1. Thus, now we discuss what happens to the optical properties of the first TLS when coupled to a series of other qubits. We assume that the coupling between the first TLS ($i = 0$) and the second one is still given by d_0 and, for simplicity, the coupling between the other TLSs is d . We also assume the same decay rate for the other TLSs, $\gamma_i = \gamma \ll \gamma_0$ ($i = 1, N$).

To understand what happens to the system when we couple more TLSs, it is instructive to analyze the eigenenergies of the bare Hamiltonian (without the probe field). When the coupling between the main and the first TLS is of the order of or weaker than its decay rate, i.e., when $d_0 \lesssim \gamma_0$, the system can present interference between the different excitation paths. This regime is represented by the gray area shown in Figs. 4(a) and 4(c). Otherwise, for $d_0 \gg \gamma_0$ the separation of the energy levels can be large enough to produce AT splitting. On the left panels of Fig. 4 we plot the first eigenenergies (ground states and eigenstates with one excitation) of the system as a function of d/γ_0 , keeping $\Omega_p = 0$ and $d_0/\gamma_0 = 0.5\gamma_0$. (See expressions

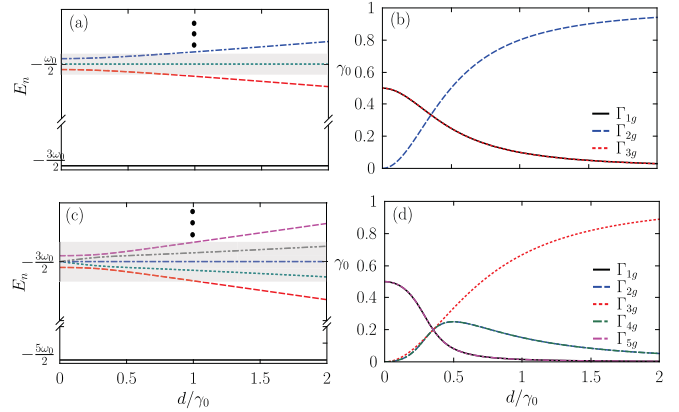


FIG. 4. (Left) First eigenenergies as a function of d/γ_0 . (Right) Transition rates from the first excited states to the ground state also as a function of d/γ_0 . In all these plots we have fixed $d_0 = 0.5\gamma_0$ and $N = 2$ in panels (a) and (b), and $N = 4$ in panels (c) and (d).

for the eigenstates and/or eigenenergies in Appendix B for the case $N = 2$.) From this figure we can see the following: (i) for $d < \gamma_0$ all the energy levels are within the linewidth of the excited state of the first TLS (γ_0); (ii) otherwise, in the intermediate region ($d \approx \gamma_0$) some levels can be inside and others outside the linewidth of the excited state, thus presenting close eigenstates with possibly different decay rates; and (iii) finally, for very strong couplings ($d_0, d \gg \gamma_0$) one observes a complete level splitting. Thus, depending on the set of parameters, the system displays total interference between the excitation paths (EIT [9]), different resonant states but, near one of each other, with asymmetric shape (Fano interference [57]), or a complete separation of the levels (AT splitting [9]).

The decay rates of the excited eigenstates $|\psi_k\rangle$ of the whole system to its ground state $|\psi_g\rangle$ can be calculated via Fermi's golden rule $\Gamma_{kg} = \gamma_0 |\langle \psi_g | \sigma_-^0 | \psi_k \rangle|^2$ [58], where we have neglected the dissipation channels related to the other TLSs since we are assuming $\gamma_0 \gg \gamma$. For a few TLSs we can analytically derive the eigenstates and then the analytical expressions for the decay rates (see Appendix B). In Figs. 4(b) ($N = 2$) and 4(d) ($N = 4$) are plotted the transition rates between the excited and ground states of the whole system as a function of coupling d for a given coupling d_0 . As can be seen, these decay rates are always different, except for a specific value of d , where all the transition rates coincide ($d = d_0/\sqrt{2}$). Such features will have a direct effect on the optical properties of the system, as discussed in the following.

In Figs. 5(a) and 5(b) we plot the absorption and dispersion of the first TLS coupled to $N = 4$ other TLSs in the DIT regime. The positions of the outer peaks depend on d_0 , while for the inner peaks their positions and widths depend on d . In this way, the number of transparency windows is exactly equal to the number of TLSs (N) coupled to the main TLS. For $d_0 < \gamma_0$ [Fig. 5(a)], we have multiple transparency windows (multi-DIT), while for $d_0, d \gg \gamma_0$ we have an AT splitting. For $d_0 < \gamma_0$ and $d > \gamma_0$ we have asymmetric excitation paths, resulting in resonant states with asymmetric line shapes [Fig. 5(b)]. This happens since the increase of the coupling d makes the

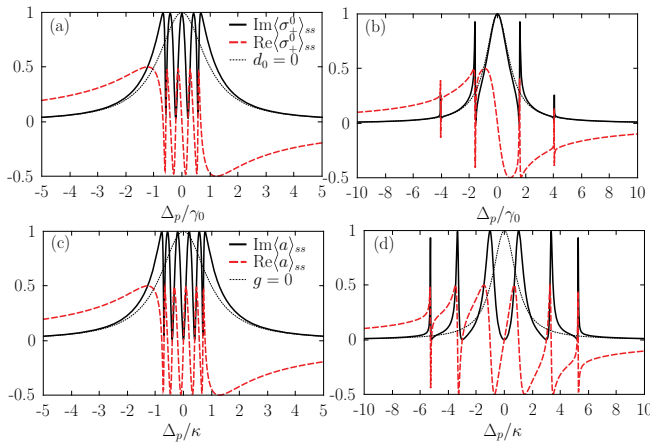


FIG. 5. Normalized absorption (black solid line) and dispersion (red dashed line) of the first TLS when coupled to $N = 4$ TLSs as a function of Δ_p/γ_0 . The parameters used here are $\Omega_p = 0.03\gamma_0$, $\gamma_i = \gamma = 10^{-3}\gamma_0$, and $d_0 = 0.5\gamma_0$. The values of the d coupling are (a) $d = d_0/\sqrt{2}$ and (b) $d = 2.5\gamma_0$. The black dotted lines represent the absorption at $d_0 = 0$. In (c) and (d) we show the normalized absorption (black solid line) and dispersion (red dashed line) of the cavity mode when coupled to five TLSs (i.e., $N = 4$) as a function of Δ_p/κ . The parameters used here are $|\epsilon| = 0.03\kappa$, $\gamma_i = \gamma = 10^{-3}\kappa$, and (c) $d = 0.4\kappa$, $g = \sqrt{2}d$, and $\gamma_0 = 10^{-3}\kappa$; and (d) $d = 3.0\kappa$, $g = 2.0\kappa$, and $\gamma_0 = 10^{-3}\kappa$. The black dotted lines represent the absorption for $g = 0$.

inner peaks broader and then, depending on the coupling d_0 , they can approach the other peaks, producing interference in the absorption paths, i.e., Fano interferences [57]. The depth of the transparency windows is strongly dependent on the decay rate γ . In Fig. 5(a) all the depths of the transparency windows are close to the maximum value since we have assumed very small γ (i.e., $\gamma = 10^{-3}\gamma_0$). On the other hand, the width of the transparency windows depend on the transition rates between the excited and ground states of the whole system. As seen in Figs. 4(b) ($N = 2$) and 4(d) ($N = 4$), all the transition rates are equal at a specific value $d = d_0/\sqrt{2}$. When they are equal, the widths of the resonance peaks of the system, which also depend on the coupling d , are the same and then we end up with perfectly symmetric multi-DIT windows.

For any number of coupled TLSs, the point where all the decay rates coincide always occurs at $d = d_0/\sqrt{2}$. (We were able to derive the decay rates and the crossing points for up to $N = 4$ TLSs coupled to the main TLS, as can be seen in Appendix B.) So, by choosing the specific parameters for that crossing point we will have a perfectly symmetrical absorption profile.

The multi-DIT or multi-Fano interference also appears when we couple the array of $1 + N$ TLSs to a cavity mode. As discussed above, the number of transparency windows is equal to the number of TLSs coupled to the main TLS. Thus, considering $1 + N$ coupled TLSs (each coupling given by d), which in turn is coupled to the cavity mode (coupling g), we will have N transparency windows, as we see in Fig. 5(c) ($N = 4$), which presents four inner peaks. The position of the resonance peaks is determined by all the couplings. However,

the outer peaks are mainly due to the atom-field coupling g , and the inner peaks (and their widths) are mainly influenced by the dipole-dipole couplings d . For greater values of g and d we can have a large separation between the resonance peaks (AT splitting) or even Fano interference when $d > g$, as we see in Fig. 5(d). So, here we have a tunable system which allows us to arbitrarily choose the number of transparency windows, and their widths, by simply adjusting the number of TLSs and the dipole-dipole coupling in our model. In Appendix C we show explicit solutions for $\langle a \rangle_{ss}$ for $N = 2$ and $N = 3$.

IV. CONCLUSIONS

In summary, here we have investigated how dipole-dipole coupling can induce transparency on a TLS or on a resonator mode. The dipole-dipole coupling works out as the control field in EIT or cavity-EIT experiments, while the decay rate of the first (second) TLS is the equivalent to the total decay rate of the excited state (the dephasing rate of the ground state which is coupled to the excited one via a control field) in EIT experiments with three-level atoms in Λ configuration. We also could show the scalability of our system: by coupling more TLSs our system presents more transparency windows, their number being exactly equal to the number of TLSs coupled to the main TLS. As mentioned before, our study can be implemented in many different physical systems. In particular, in Ref. [43] we find a very good platform to experimentally investigate our results, since it presents a controllable coupling between two different two-level systems: the Josephson-phase qubit and the atoms which can occupy two different states (positions). Additionally, the states of the atomic system present much longer coherence times than those from the superconducting qubits, which is another requirement for the observation of the dipole-induced transparency predicted in our work. Likewise, in Ref. [45] was observed a dark state with a long lifetime, occasioned by the interaction of a flux qubit with a couple of nitrogen vacancy ensembles in a diamond hybrid system. The signature of this dark state is related to the experimental observation of a narrow peak at the crossing point of levels in the energy spectrum. Thus, those results are very connected to those we present here, making the system of Ref. [45] another suitable platform to investigate the phenomena predicted in our work. We hope this kind of induced transparency could be useful for manipulation of the optical properties of TLSs in general, for example, for the study of slow light, transport properties in spin chains, and also frequency filters for light fields. Also, by detecting the optical response of a driven TLS or resonator mode we can estimate properties of dipole-dipole interaction.

ACKNOWLEDGMENTS

C.J.V.-B. and H.S.B. acknowledge support from São Paulo Research Foundation (FAPESP), Grants No. 2013/04162-5 and No. 2014/12740-1, and the Brazilian National Institute of Science and Technology for Quantum Information (INCT-IQ), Grant No. 465469/2014-0. C.J.V.-B. and E.C.D. acknowledge support from CNPq, Grants No. 308860/2015-2 and No. 161117/2014-7.

APPENDIX A: 1 + N COUPLED TLSS IN FREE SPACE

In this first part we demonstrate some expressions for a stationary solution of the $\langle \sigma_-^0 \rangle_{ss}$ for 1 + N coupled TLSs (with dipole-dipole interaction) in free space. Assuming a low atomic excitation limit, the linear response of our system and of the usual three-level system where the EIT phenomenon is observed (given by imaginary and real parts of the first-order optical susceptibility function $\chi^{(1)}$) are completely analogous, as can be seen in the expressions below:

$$\chi_{DIT}^{(1)} = \frac{\Delta_p + i\gamma_1}{d_0^2 + (\gamma_0 - i\Delta_p)(\gamma_1 - i\Delta_p)}, \quad (A1)$$

$$\chi_{EIT}^{(1)} = \frac{\Delta_p}{\Omega_c^2 - \Delta_p(\Delta_p + i\Gamma_3)}, \quad (A2)$$

being $\Gamma_3 = \Gamma_{31} + \Gamma_{32}$. Therefore, with $\gamma_1 = 0$, $\gamma_0 \rightarrow \Gamma_3$, and $d_0 \rightarrow \Omega_c$ the expressions are exactly the same.

On the other hand, the nonlinear terms of the optical susceptibility function present a significant difference. This feature can be clearly seen in the third order of the optical susceptibility function, whose expressions for both systems are given by

$$\chi_{DIT}^{(3)} = \frac{2i[-(\gamma_1 - i\Delta_p)^2(\gamma_1 + i\Delta_p)(\gamma_0 + \gamma_1 - 2i\Delta_p) + d_0^4 + d_0^2(\gamma_1^2 + \Delta_p^2)]}{(\gamma_0 + \gamma_1 - 2i\Delta_p)[d_0^2 + (\gamma_0 - i\Delta_p)(\gamma_1 - i\Delta_p)]^2[d_0^2 + (\gamma_0 + i\Delta_p)(\gamma_1 + i\Delta_p)]}, \quad (A3)$$

$$\chi_{EIT}^{(3)} = \frac{\Delta_p\{-i\Gamma_{32}\Delta_p^2\Gamma_3^2 + \Delta_p\Omega_c^2[\Gamma_{32}\Gamma_3 - i\Delta_p(2\Gamma_{31} + 3\Gamma_{32})] - 2i\Gamma_{31}\Omega_c^4\}}{\Gamma_{31}[\Delta_p(\Gamma_3 + i\Delta_p) - i\Omega_c^2][\Delta_p\Omega_c(\Gamma_3 - i\Delta_p) + i\Omega_c^3]^2}. \quad (A4)$$

In order to make evident the difference in the optical response of both systems, the optical response is shown in Fig. 2 of the main text (real and imaginary parts of the χ function) for the two systems: two TLSs coupled by dipole-dipole interaction and for a three-level system in the Λ configuration. From these results we can clearly see, in the limit of a weak probe field, the linear optical response is equal for both systems. However, the nonlinear response (as $\chi^{(3)}$) presents significant difference.

From the general solution shown in the main text (3) one can derive the stationary solution for an arbitrary number of coupled TLSs. For instance, below we present some explicit expressions. For $N = 2$ the solution is

$$\langle \sigma_+^0 \rangle_{ss} = -\frac{\Omega_p[d^2 - (\Delta_p + i\gamma_1)(\Delta_p + i\gamma_2)]}{(\Delta_p + i\gamma_0)[d^2 - (\Delta_p + i\gamma_1)(\Delta_p + i\gamma_2)] + d_0^2(\Delta_p + i\gamma_2)}.$$

The stationary solution for $N = 3$ is

$$\langle \sigma_+^0 \rangle_{ss} = \frac{i\Omega_p\{id^2(\Delta_p + i\gamma_3) + (\gamma_1 - i\Delta_p)[-d^2 + (\Delta_p + i\gamma_2)(\Delta_p + i\gamma_3)]\}}{d_0^2[-d^2 + (\Delta_p + i\gamma_2)(\Delta_p + i\gamma_3)] + (\Delta_p + i\gamma_0)\{d^2(\Delta_p + i\gamma_3) - (\Delta_p + i\gamma_1)[-d^2 + (\Delta_p + i\gamma_2)(\Delta_p + i\gamma_3)]\}}.$$

For $N = 4$, the solution in the steady state is given by

$$\langle \sigma_+^0 \rangle_{ss} = \frac{i\Omega_p\{d^2[-d^2 + (\Delta_p + i\gamma_3)(\Delta_p + i\gamma_4)] + (\Delta_p + i\gamma_1)\{d^2(\Delta_p + i\gamma_4) + (-\Delta_p - i\gamma_2)[-d^2 + (\Delta_p + i\gamma_3)(\Delta_p + i\gamma_4)]\}\}}{d_0^2\{id^2(\Delta_p + i\gamma_4) + (\gamma_2 - i\Delta_p)[-d^2 + (\Delta_p + i\gamma_3)(\Delta_p + i\gamma_4)]\} + \Upsilon},$$

where

$$\Upsilon = (\Delta_p + i\gamma_0)(d^2[(\gamma_3 - i\Delta_p)(\Delta_p + i\gamma_4) + id^2] + (\Delta_p + i\gamma_1)\{d^2(\gamma_4 - i\Delta_p) + i(\Delta_p + i\gamma_2)[-d^2 + (\Delta_p + i\gamma_3)(\Delta_p + i\gamma_4)]\})$$

Just to illustrate, in Fig. 6 we present the absorption spectrum for $N = 7, 10, 12$, and 15. Note that the number of transparency windows is exactly equal to N . Also, note that the depth of the transparency windows is different in this figure. This is due to the non-null decay rate γ used here. By increasing the number of TLSs coupled to the main TLS, we increase the number of transparency windows. However, the higher the number of transparency windows, the more sensitive the system is to the noisy effects.

APPENDIX B: EIGENSTATES, EIGENENERGIES, AND TRANSITION RATES BETWEEN THE FIRST EXCITED STATES AND THE GROUND STATE FOR 1 + N TLSS

The main goal of this section is to present the analytical solutions for the transition rates between the eigenstates of the system (the first excited state and the ground state). To this end, first we must derive the eigenstates of our system, once the transition

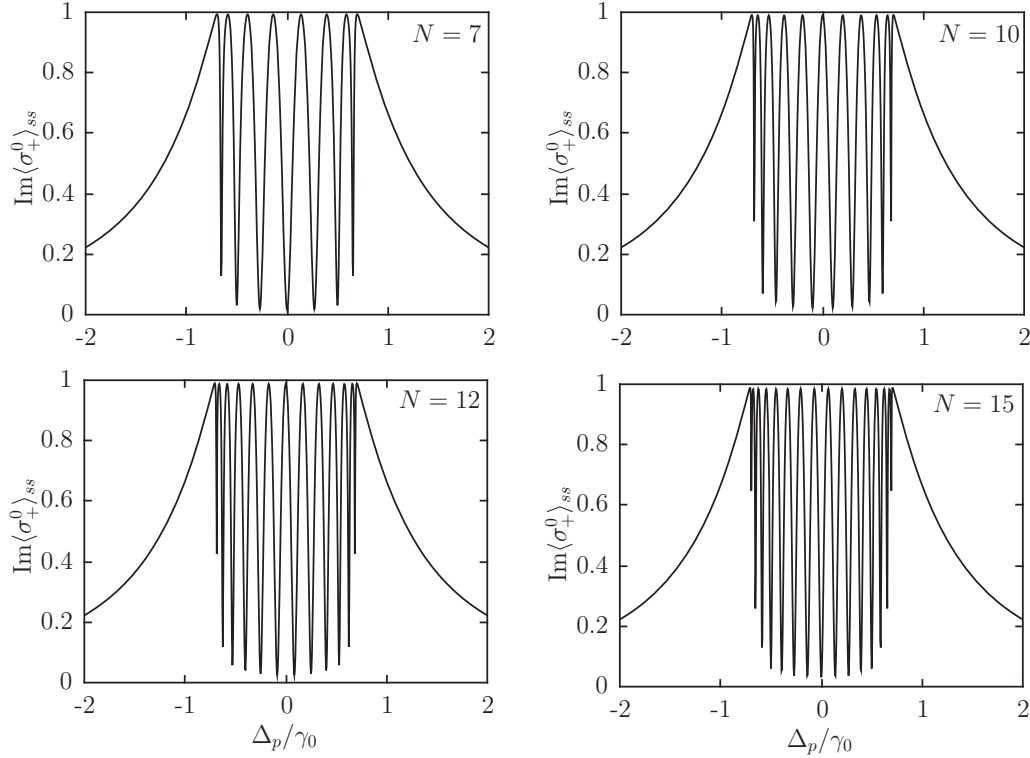


FIG. 6. Normalized absorption $\text{Im}(\sigma_{+}^0)_{ss}$ as a function of the normalized detuning Δ_p/γ_0 for different numbers of TLSs coupled to the main one ($N = 7, 10, 12$, and 15). The parameters used here were $\gamma_0 = 1$, $\Omega_p = 0.03\gamma_0$, $\gamma_i = \gamma = 10^{-3}\gamma_0$, $d_0 = 0.5\gamma_0$, and $d = d_0/\sqrt{2}$.

rate is defined as

$$\Gamma_{kg} = \gamma_0 |\langle \psi_g | \sigma_-^0 | \psi_k \rangle|^2, \quad (\text{B1})$$

$|\psi_g\rangle$ and $|\psi_k\rangle$ ($k = 1, 2, \dots$) being the ground and excited eigenstates, respectively.

We have obtained analytically the expressions for the eigenstates and transition rates for $N = 2, 3$, and 4 only. As the expressions for the eigenstates or eigenenergies are too extensive, below we present them only for the $N = 2$ case.

For $N = 2$, the eigenvalues and the respective eigenvectors are

$$\begin{aligned} E_0 &= -3\omega_0 \rightarrow |\psi_0\rangle = |ggg\rangle, \\ E_1 &= -\omega_0 - \sqrt{d_0^2 + d^2} \rightarrow |\psi_1\rangle = \frac{d_0}{\sqrt{2(d_0^2 + d^2)}} |egg\rangle - \frac{1}{\sqrt{2}} |geg\rangle + \frac{d}{\sqrt{2(d_0^2 + d^2)}} |gge\rangle, \\ E_2 &= -\omega_0 \rightarrow |\psi_2\rangle = -\frac{d}{\sqrt{d_0^2 + d^2}} |egg\rangle + \frac{d_0}{\sqrt{d_0^2 + d^2}} |gge\rangle, \\ E_3 &= -\omega_0 + \sqrt{d_0^2 + d^2} \rightarrow |\psi_3\rangle = \frac{d_0}{\sqrt{2(d_0^2 + d^2)}} |egg\rangle + \frac{1}{\sqrt{2}} |geg\rangle + \frac{d}{\sqrt{2(d_0^2 + d^2)}} |gge\rangle, \\ E_4 &= \omega_0 - \sqrt{d_0^2 + d^2} \rightarrow |\psi_4\rangle = \frac{d}{\sqrt{2(d_0^2 + d^2)}} |eeg\rangle - \frac{1}{\sqrt{2}} |ege\rangle + \frac{d_0}{\sqrt{2(d_0^2 + d^2)}} |gee\rangle, \\ E_5 &= \omega_0 \rightarrow |\psi_5\rangle = -\frac{d_0}{\sqrt{d_0^2 + d^2}} |eeg\rangle + \frac{d}{\sqrt{d_0^2 + d^2}} |gee\rangle, \\ E_6 &= \omega_0 + \sqrt{d_0^2 + d^2} \rightarrow |\psi_6\rangle = \frac{d}{\sqrt{2(d_0^2 + d^2)}} |eeg\rangle + \frac{1}{\sqrt{2}} |ege\rangle + \frac{d_0}{\sqrt{2(d_0^2 + d^2)}} |gee\rangle, \\ E_7 &= 3\omega_0 \rightarrow |\psi_7\rangle = |eee\rangle. \end{aligned}$$

With those eigenstates we can derive the transition rates between the first excited states (with one excitation) and the ground state, which reads

$$\Gamma_{2g} = \frac{d^2}{d_0^2 + d^2}, \quad \Gamma_{1g} = \Gamma_{3g} = \frac{d_0^2}{2(d^2 + d_0^2)}.$$

From these expressions we find that these transition rates have a crossing point at $d = \frac{d_0}{\sqrt{2}}$.

For $N = 3$, the transition rates are given by

$$\Gamma_{2g} = \Gamma_{3g} = \frac{2d^2 - d_0^2 + \sqrt{4d^2 + d_0^2}}{4\sqrt{4d^2 + d_0^2}}, \quad \Gamma_{1g} = \Gamma_{4g} = \frac{-2d^2 + d_0^2 + \sqrt{4d^2 + d_0^2}}{4\sqrt{4d^2 + d_0^2}},$$

and the crossing point of the transition rates is exactly the same, $d = \frac{d_0}{\sqrt{2}}$.

For $N = 4$, the expressions of transition rates follow below:

$$\Gamma_{3g} = \frac{d^2}{d^2 + 2d_0^2}, \quad \Gamma_{2g} = \Gamma_{4g} = \frac{d_0^2(2d^2 - d_0^2 + C)}{2(d^2 + 2d_0^2)C}, \quad \Gamma_{1g} = \Gamma_{5g} = \frac{d_0^2(-2d^2 + d_0^2 + C)}{2(d^2 + 2d_0^2)C},$$

where $C = \sqrt{5d^4 - 2d^2d_0^2 + d_0^4}$. For this configuration we have found two crossing points: $d = \frac{d_0}{\sqrt{2}}$, in which all the rates cross, and $d = \sqrt{\frac{2}{3}}d_0$, where some rates cross.

APPENDIX C: TLSs COUPLED TO A RESONATOR – ANALYTICAL SOLUTIONS

Here we consider $1 + N$ coupled TLSs with the first one interacting with a resonator (for instance, in the circuit QED framework). From the general solution shown in the main text (10) we also can obtain the expression for the expected value to $\langle a \rangle$ in steady state for any number of TLSs coupled to the resonator. For instance, below we show some explicit expressions for $\langle a \rangle_{ss}$. For $N = 2$ it reads

$$\langle a \rangle_{ss} = - \left\{ \frac{\epsilon \{d^2(-i\gamma_2 + \Delta_p) + (-i\gamma_0 + \Delta_p)[d^2 - (-i\gamma_1 + \Delta_p)(-i\gamma_2 + \Delta_p)]\}}{-g^2[d^2 - (-i\gamma_1 + \Delta_p)(-i\gamma_2 + \Delta_p)] + \{d^2(-i\gamma_2 + \Delta_p) + (-i\gamma_0 + \Delta_p)[d^2 - (-i\gamma_1 + \Delta_p)(-i\gamma_2 + \Delta_p)]\}(-i\kappa + \Delta_p)} \right\}.$$

For $N = 3$ we obtain to steady state the solution

$$\langle a \rangle_{ss} = - \left\{ \frac{-\epsilon(-d^2[d^2 - (-i\gamma_2 + \Delta_p)(-i\gamma_3 + \Delta_p)] + (-i\gamma_0 + \Delta_p)\{d^2(-i\gamma_3 + \Delta_p) + (-i\gamma_1 + \Delta_p)[d^2 - (-i\gamma_2 + \Delta_p)(-i\gamma_3 + \Delta_p)]\}}{-g^2\{d^2(-i\gamma_3 + \Delta_p) + (-i\gamma_1 + \Delta_p)[d^2 - (-i\gamma_2 + \Delta_p)(-i\gamma_3 + \Delta_p)]\} + \Psi_a} \right\},$$

with

$$\Psi_a = \{-d^2[d^2 - (-i\gamma_2 + \Delta_p)(-i\gamma_3 + \Delta_p)] + (-i\gamma_0 + \Delta_p)\{d^2(-i\gamma_3 + \Delta_p) + (-i\gamma_1 + \Delta_p) \times [d^2 - (-i\gamma_2 + \Delta_p)(-i\gamma_3 + \Delta_p)]\}(-i\kappa + \Delta_p)\}.$$

Again, we were able to derive the steady-state analytical solutions for arbitrary N 's, but the expressions are very large to be presented here. Just to illustrate, in Fig. 7 we present the absorption spectrum for $N = 7, 10, 12$, and 15. Note that the number of transparency windows exactly equals N .

Transition rates between the first excited states to the ground state for $1 + N$ TLSs coupled to a resonator mode

Analogous to the free-space case, we could derive the transition rates for some cases when $1 + N$ TLSs are coupled to the resonator. It can be calculated through the following expression:

$$\Gamma_{kg} = \gamma_0 |\langle \psi_g | a | \psi_k \rangle|^2,$$

$|\psi_g\rangle$ and $|\psi_k\rangle$ ($k = 1, 2, \dots$) being the ground and excited eigenstates, respectively.

For $N = 2$, the rates are given by

$$\Gamma_{1g} = \Gamma_{4g} = \frac{d^2 g^2}{4d^4 + g^4 + (2d^2 - g^2)\sqrt{4d^4 + g^4}}, \quad \Gamma_{2g} = \Gamma_{3g} = \frac{d^2 g^2}{4d^4 + g^4 + (g^2 - 2d^2)\sqrt{4d^4 + g^4}}.$$

Similarly to what happens in the free space, there is a crossing point associated to a specific value of d where all the transition rates are the same. For this case the crossing point is $d = g/\sqrt{2}$.

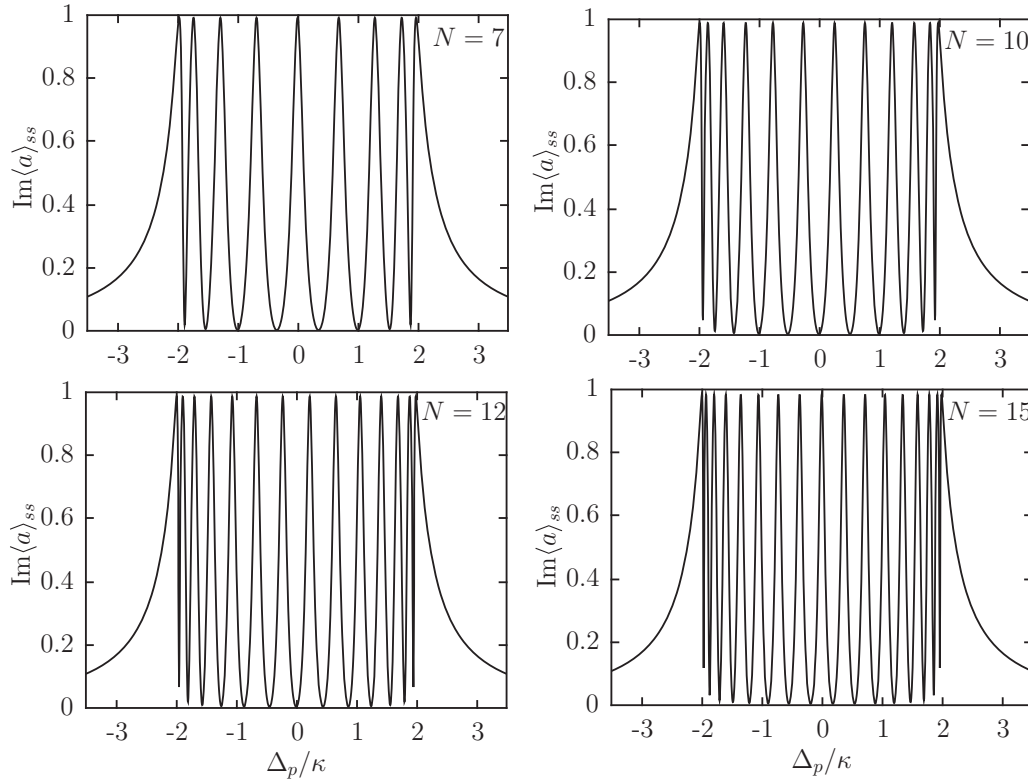


FIG. 7. Normalized transmission $\text{Im}\langle a \rangle_{ss}$ as a function of the normalized detuning Δ_p/κ for $1 + N$ TLSs coupled to the cavity mode (for $N = 7, 10, 12$, and 15). The parameters used here are $\gamma_0 = \gamma_i = 10^{-3}\kappa$, $|\epsilon| = 0.03\kappa$, $d = 1.0\kappa$, and $g = \sqrt{2}d$.

For $N = 3$, the rates are given by

$$\Gamma_{3g} = \frac{d^2}{d^2 + 2g^2}, \quad \Gamma_{1g} = \Gamma_{5g} = \frac{g^2(g^2 - 2d^2 + C)}{2C(d^2 + 2g^2)}, \quad \Gamma_{2g} = \Gamma_{4g} = \frac{g^2(2d^2 - g^2 + C)}{2C(d^2 + 2g^2)},$$

with $C = \sqrt{5d^4 - 2d^2g^2 + g^4}$. For this case all the rates cross again at $d = g/\sqrt{2}$, while some rates cross at $d = \sqrt{2/5}g$.

-
- [1] B. E. Kane, A silicon-based nuclear spin quantum computer, *Nature (London)* **393**, 133 (1998).
- [2] T. D. Ladd, F. Jelezko, R. Laflamme, Y. Nakamura, C. Monroe, and J. L. O'Brien, Quantum computers, *Nature (London)* **464**, 45 (2010).
- [3] M. Gross and S. Haroche, Superradiance: An essay on the theory of collective spontaneous emission, *Phys. Rep.* **93**, 301 (1982).
- [4] D. Leibfried, R. Blatt, C. Monroe, and D. Wineland, Quantum dynamics of single trapped ions, *Rev. Mod. Phys.* **75**, 281 (2003).
- [5] A. Reiserer and G. Rempe, Cavity-based quantum networks with single atoms and optical photons, *Rev. Mod. Phys.* **87**, 1379 (2015).
- [6] Z.-L. Xiang, S. Ashhab, J. Q. You, and F. Nori, Hybrid quantum circuits: Superconducting circuits interacting with other quantum systems, *Rev. Mod. Phys.* **85**, 623 (2013).
- [7] L.-M. Duan and C. Monroe, Colloquium: Quantum networks with trapped ions, *Rev. Mod. Phys.* **82**, 1209 (2010).
- [8] K.-J. Boller, A. Imamoglu, and S. E. Harris, Observation of Electromagnetically Induced Transparency, *Phys. Rev. Lett.* **66**, 2593 (1991).
- [9] M. Fleischhauer, A. Imamoglu, and J. P. Marangos, Electromagnetically induced transparency: Optics in coherent media, *Rev. Mod. Phys.* **77**, 633 (2005).
- [10] S. Parkins, Quantum optics: Single-atom transistor for light, *Nature (London)* **465**, 699 (2010).
- [11] M. Mücke, E. Figueroa, J. Bochmann, C. Hahn, K. Murr, S. Ritter, C. J. Villas-Boas, and G. Rempe, Electromagnetically induced transparency with single atoms in a cavity, *Nature (London)* **465**, 755 (2010).
- [12] K. S. Choi, H. Deng, J. Laurat, and H. J. Kimble, Mapping photonic entanglement into and out of a quantum memory, *Nature (London)* **452**, 67 (2008).
- [13] H. P. Specht, C. Nolleke, A. Reiserer, M. Uphoff, E. Figueroa, S. Ritter, and G. Rempe, A single-atom quantum memory, *Nature (London)* **473**, 190 (2011).
- [14] H. S. Borges and C. J. Villas-Boas, Quantum phase gate based on electromagnetically induced transparency in optical cavities, *Phys. Rev. A* **94**, 052337 (2016).
- [15] G. Morigi, J. Eschner, and C. H. Keitel, Ground State Laser Cooling Using Electromagnetically Induced Transparency, *Phys. Rev. Lett.* **85**, 4458 (2000).

- [16] C. F. Roos, D. Leibfried, A. Mundt, F. Schmidt-Kaler, J. Eschner, and R. Blatt, Experimental Demonstration of Ground State Laser Cooling with Electromagnetically Induced Transparency, *Phys. Rev. Lett.* **85**, 5547 (2000).
- [17] R. Lechner, C. Maier, C. Hempel, P. Jurcevic, B. P. Lanyon, T. Monz, M. Brownnutt, R. Blatt, and C. F. Roos, Electromagnetically-induced-transparency ground-state cooling of long ion strings, *Phys. Rev. A* **93**, 053401 (2016).
- [18] C. L. Garrido-Alzar, M. A. G. Martinez, and P. Nussenzveig, Classical analog of electromagnetically induced transparency, *Am. J. Phys.* **70**, 37 (2002).
- [19] M. A. de Ponte, C. J. Villas-Boas, R. M. Serra, and M. H. Y. Moussa, Electromagnetically induced transparency and dynamic Stark effect in coupled quantum resonators, *Europhys. Lett.* **72**, 383 (2005).
- [20] Q. Xu, S. Sandhu, M. L. Povinelli, J. Shakya, S. Fan, and M. Lipson, Experimental Realization of an On-Chip All-Optical Analogue to Electromagnetically Induced Transparency, *Phys. Rev. Lett.* **96**, 123901 (2006).
- [21] J. A. Souza, L. Cabral, R. R. Oliveira, and C. J. Villas-Boas, Electromagnetically-induced-transparency-related phenomena and their mechanical analogs, *Phys. Rev. A* **92**, 023818 (2015).
- [22] P. R. Rice and R. J. Brecha, Cavity induced transparency, *Opt. Commun.* **126**, 230 (1996).
- [23] E. Waks and J. Vuckovic, Dipole Induced Transparency in Drop-Filter Cavity-Waveguide Systems, *Phys. Rev. Lett.* **96**, 153601 (2006).
- [24] C.-H. Yuan and K.-D. Zhu, Voltage-controlled slow light in asymmetry double quantum dots, *Appl. Phys. Lett.* **89**, 052115 (2006).
- [25] H. S. Borges, L. Sanz, J. M. Villas-Bôas, O. O. Diniz Neto, and A. M. Alcalde, Tunneling induced transparency and slow light in quantum dot molecules, *Phys. Rev. B* **85**, 115425 (2012).
- [26] H. S. Borges, M. H. Oliveira, and C. J. Villas-Boas, Influence of the asymmetric excited state decay on coherent population trapping, *Sci. Rep.* **7**, 7132 (2017).
- [27] N. Liu, L. Langguth, T. Weiss, J. Kaste, M. Fleischhauer, T. Pfau, and H. Giessen, Plasmonic analog of electromagnetically induced transparency at the Drude damping limit, *Nat. Mater.* **8**, 758 (2009).
- [28] H. Lu, X. Liu, and D. Mao, Plasmonic analog of electromagnetically induced transparency in multi-nanoresonator-coupled waveguide systems, *Phys. Rev. A* **85**, 053803 (2012).
- [29] S. Weis, R. Riviere, S. Deleglise, E. Gavartin, O. Arcizet, A. Schliesser, and T. J. Kippenberg, Optomechanically induced transparency, *Science* **330**, 1520 (2010).
- [30] A. Sohail, Y. Zhang, J. Zhang, and C.-S. Yu, Optomechanically induced transparency in multi-cavity optomechanical system with and without one two-level atom, *Sci. Rep.* **6**, 28830 (2016).
- [31] N. Papanikolaou, V. A. Fedotov, N. I. Zheludev, and S. L. Prosvirnin, Metamaterial Analog of Electromagnetically Induced Transparency, *Phys. Rev. Lett.* **101**, 253903 (2008).
- [32] P. Tassin, L. Zhang, T. Koschny, E. N. Economou, and C. M. Soukoulis, Planar designs for electromagnetically induced transparency in metamaterials, *Opt. Express* **17**, 5595 (2009).
- [33] M. D. Lukin, S. F. Yelin, M. Fleischhauer, and M. O. Scully, Quantum interference effects induced by interacting dark resonances, *Phys. Rev. A* **60**, 3225 (1999).
- [34] S. Li, X. Yang, X. Cao, C. Xie, and H. Wang, Two electromagnetically induced transparency windows and an enhanced electromagnetically induced transparency signal in a four-level tripod atomic system, *J. Phys. B* **40**, 3211 (2007).
- [35] X. Yang, M. Yu, D.-L. Kwong, and C. W. Wong, All-Optical Analog to Electromagnetically Induced Transparency in Multiple Coupled Photonic Crystal Cavities, *Phys. Rev. Lett.* **102**, 173902 (2009).
- [36] P.-C. Ma, J.-Q. Zhang, Y. Xiao, M. Feng, and Z.-M. Zhang, Tunable double optomechanically induced transparency in an optomechanical system, *Phys. Rev. A* **90**, 043825 (2014).
- [37] E. Paspalakis and P. L. Knight, Electromagnetically induced transparency and controlled group velocity in a multilevel system, *Phys. Rev. A* **66**, 015802 (2002).
- [38] Y.-F. Xiao, X.-B. Zou, W. Jiang, Y.-L. Chen, and G.-C. Guo, Analog to multiple electromagnetically induced transparency in all-optical drop-filter systems, *Phys. Rev. A* **75**, 063833 (2007).
- [39] L.-M. Duan, E. Demler, and M. D. Lukin, Controlling Spin Exchange Interactions of Ultracold Atoms in Optical Lattices, *Phys. Rev. Lett.* **91**, 090402 (2003).
- [40] J. J. Garcia-Ripoll, M. A. Martin-Delgado, and J. I. Cirac, Implementation of Spin Hamiltonians in Optical Lattices, *Phys. Rev. Lett.* **93**, 250405 (2004).
- [41] C. Joshi, F. Nissen, and J. Keeling, Quantum correlations in the one-dimensional driven dissipative XY model, *Phys. Rev. A* **88**, 063835 (2013).
- [42] R. W. Simmonds, K. M. Lang, D. A. Hite, S. Nam, D. P. Pappas, and J. M. Martinis, Decoherence in Josephson Phase Qubits from Junction Resonators, *Phys. Rev. Lett.* **93**, 077003 (2004).
- [43] M. Neeley, M. Ansmann, R. C. Bialczak, M. Hofheinz, N. Katz, E. Lucero, A. O'Connell, H. Wang, A. N. Cleland, and J. M. Martinis, Process tomography of quantum memory in a Josephson-phase qubit coupled to a two-level state, *Nat. Phys.* **4**, 523 (2008).
- [44] J. Lisenfeld, C. Muller, J. H. Cole, P. Bushev, A. Lukashenko, A. Shnirman, and A. V. Ustinov, Measuring the Temperature Dependence of Individual Two-Level Systems by Direct Coherent Control, *Phys. Rev. Lett.* **105**, 230504 (2010).
- [45] X. Zhu, Y. Matsuzaki, R. Amsüss, K. Kakuyanagi, T. Shimooka, N. Mizuochi, K. Nemoto, K. Semba, W. J. Munro, and S. Saito, Observation of dark states in a superconductor diamond quantum hybrid system, *Nat. Commun.* **5**, 3524 (2014).
- [46] J. Lisenfeld, G. J. Grabovskij, C. Muller, J. H. Cole, G. Weiss, and A. V. Ustinov, Observation of directly interacting coherent two-level systems in an amorphous material, *Nat. Commun.* **6**, 6182 (2015).
- [47] Y. Salathe, M. Mondal, M. Oppliger, J. Heinsoo, P. Kurpiers, A. Potocnik, A. Mezzacapo, U. Las Heras, L. Lamata, E. Solano, S. Filipp, and A. Wallraff, Digital Quantum Simulation of Spin Models with Circuit Quantum Electrodynamics, *Phys. Rev. X* **5**, 021027 (2015).
- [48] R. Blatt and C. F. Roos, Quantum simulations with trapped ions, *Nat. Phys.* **8**, 277 (2012).
- [49] A. N. Al-Ahmadi and S. E. Ulloa, Extended coherent exciton states in quantum dot arrays, *Appl. Phys. Lett.* **88**, 043110 (2006).
- [50] D. M. Zajac, T. M. Hazard, X. Mi, E. Nielsen, and J. R. Petta, Scalable Gate Architecture for a One-Dimensional Array of Semiconductor Spin Qubits, *Phys. Rev. Appl.* **6**, 054013 (2016).

- [51] H.-P. Breuer and F. Petruccione, *The Theory of Open Quantum Systems* (Oxford University Press, Oxford, UK, 2007).
- [52] H. J. Carmichael, L. Tian, W. Ren, and P. Alsing, in *Cavity Quantum Electrodynamics*, edited by P. R. Berman (Academic Press, Boston, MA, 1994).
- [53] J. Gea-Banacloche, M. Mumba, and M. Xiao, Optical switching in arrays of quantum dots with dipole-dipole interactions, *Phys. Rev. B* **74**, 165330 (2006).
- [54] P. M. Anisimov, J. P. Dowling, and B. C. Sanders, Objectively Discerning Autler-Townes Splitting from Electromagnetically Induced Transparency, *Phys. Rev. Lett.* **107**, 163604 (2011).
- [55] R. Puthumpally-Joseph, M. Sukharev, O. Atabek, and E. Charon, Dipole-Induced Electromagnetic Transparency, *Phys. Rev. Lett.* **113**, 163603 (2014).
- [56] Considering two coupled dipoles, as discussed in the main text, the decay rate of the second dipole plays the role of the dephasing rate in usual EIT experiments with three-level atoms in Λ -level configuration. Only in the limit of a very small dephasing rate can we observe narrow transparency windows ($\text{FWHM} < \gamma_0$), which is typical from EIT experiments. By assuming the same decay rate γ_0 for both dipoles, as done in [55], we would see transparency only in the strong dipole coupling (d) regime, i.e., for $d \gg \gamma_0$. But in this limit we have an Autler-Townes splitting rather than EIT phenomenon. In fact, the FWHM of the transparency window observed in [55] is much wider than the dipole linewidth.
- [57] U. Fano, Effects of configuration interaction on intensities and phase shifts, *Phys. Rev.* **124**, 1866 (1961).
- [58] C. Cohen-Tannoudji, J. Dupont-Roc, and G. Grynberg, *Atom-Photon Interactions* (Wiley, New York, 1992).